Document No.: TRPCS- ATBD-035

Time-Resolved Observations of Precipitation structure and storm Intensity with a Constellation of Smallsats

Level-2A Unified Resolution Radiometric Product Algorithm Theoretical Basis Document

12 January 2022

Revision 2.1

National Aeronautics and Space Administration
Goddard Earth Science Data Information and Services Center (GES DISC)

This material is based upon work supported by the National Aeronautics and Space Administration under Air Force Contract No. FA8702-15-D-0001. Any opinions, findings, conclusions or recommendations expressed in this material are those of the author(s) and do not necessarily reflect the views of the National Aeronautics and Space Administration .

Prepared by: Ralf Bennartz Date: _____
Vanderbilt University & University of Wisconsin - Madison

Approved by: _____ Date: _____
William J. Blackwell
TROPICS Principal Investigator
MIT Lincoln Laboratory

Approved by: _____ Date: _____
Scott Braun
TROPICS Project Scientist
NASA Goddard Space Flight Center

Approved by: _____ Date: _____
R. Vincent Leslie
TROPICS Project Manager
MIT Lincoln Laboratory

LINCOLN LABORATORY
MASSACHUSETTS INSTITUTE OF TECHNOLOGY

Revision History

Version	*Description*	*Date*	*Initiator*
1.0	Initial Draft	07/20/2017	Ralf Bennartz
2.0	Revised Draft	12/28/2019	Ralf Bennartz
2.1	Added updated polarization information	01/12/2022	Vince Leslie

Contents

1 Scope

This Algorithm Theoretical Basis Document (ATBD) describes the theoretical background of the TROPICS Level-2A Unified Resolution Radiometric product (L2A-URRP). It also includes TROPICS payload characteristics and the algorithm's ancillary data (i.e., data coming from sources other than the TROPICS Space Vehicle). Details of the L2A-URRP data product format can be found in the TROPICS Data User's Guide. This ATBD will also contain the pre-launch testing completed to verify the algorithm. The TROPICS Data User's Guide will contain the post-launch validation.

2 System Overview

The Time-Resolved Observations of Precipitation structure and storm Intensity with a Constellation of Smallsats (TROPICS) mission [1] will provide rapid-refresh microwave measurements over the tropics that can be used to observe the thermodynamics of the troposphere and precipitation structure for storm systems at the mesoscale and synoptic scale over the entire storm lifecycle. TROPICS comprises a constellation of six CubeSats in three low-Earth orbital planes. Each CubeSat will host a high-performance radiometer scanning across the satellite track at 30 RPM to provide temperature profiles using seven channels near the 118.75 GHz oxygen absorption line, water vapor profiles using 3 channels near the 183 GHz water vapor absorption line, imagery in a single channel near 90 GHz for precipitation measurements, and a single channel at 206 GHz for cloud ice measurements. This observing system offers an unprecedented combination of horizontal and temporal resolution to measure environmental and inner-core conditions for tropical cyclones (TCs) on a nearly global scale and is a profound leap forward in the temporal resolution of several key parameters needed for detailed study of high-impact meteorological events (e.g., Tropical Cyclones). TROPICS will demonstrate that a constellation approach to earth Science can provide improved resolution, configurable coverage (tropics, near global, or global), flexibility, reliability, and launch access at extremely cost effective, thereby serving as a model for future missions.

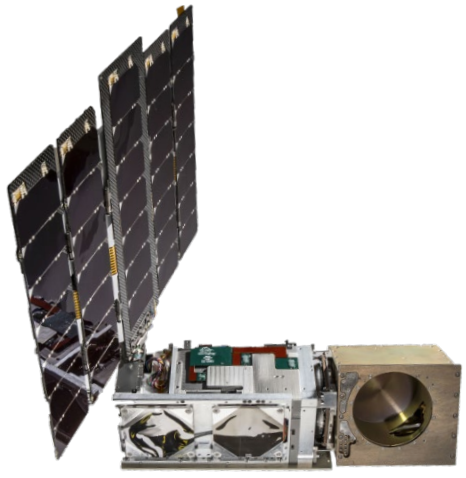

Figure 1 Photo of TROPICS Space Vehicle

3 Applicable TROPICS Documents

1. TROPICS Data Product User Guide: Publicly released document with information on payload and space vehicle characteristics, quality flags, and validation along with full data product format description.
2. TROPICS Radiometric Calibration ATBD (Level-1a and Level-1b data products)
3. TROPICS Atmospheric Vertical Profiles ATBD containing the Atmospheric Vertical Profile Temperature Profile (AVTP) and Atmospheric Vertical Moisture Profile (AVMP) ATBD (Level-2b data products) using NOAA MIRS algorithm
4. TROPICS Instantaneous Surface Rain Rate (ISRR) ATBD (Level-2b data product) using the Goddard NASA PRPS algorithm
5. TROPICS Tropical Cyclone Intensity ATBD (Level-2b data product consisting of Minimum Sea-Level Pressure and Maximum Sustained Wind Speed)

4 Payload Characteristics

This section presents the TROPICS payload characteristics. The payload is a total-power radiometer with channels at W, F, and G bands.

4.1 Receiver Architecture

Table 1 contains the spectral passbands, spatial beamwidth, and expected Noise Equivalent Delta Noise (NEdT) of the channels. TROPICS weighting functions can be found in the TROPICS Level-2b AVP ATBD. Each SV's NEDT can be found in Appendix A: Noise Equivalent Delta Noise. A complete list of individual beamwidths can be found in Appendix B: Antenna Pattern Beamwidths (Full-width Half Max.).

Table 1 TROPICS spectral and spatial Stats (Footprint from 550-km altitude)

Chan.	Center Freq. (GHz)	Band width (GHz)	RF Span (GHz)	Beamwidth (degrees) Down/Cross	Nadir Footprint Geometric Mean (km)
1	91.655 ± 1.4	1.000	89.756-90.756, 92.556-93.556	3.0/3.17	29.6
2	114.50	1.000	114.00-115.00	2.4/2.62	24.1
3	115.95	0.800	115.55-116.35	2.4/2.62	24.1
4	116.65	0.600	116.35-116.95	2.4/2.62	24.1
5	117.25	0.600	116.95-117.55	2.4/2.62	24.1

6	117.80	0.500	117.55-118.05	2.4/2.62	24.1
7	118.24	0.380	118.05-118.43	2.4/2.62	24.1
8	118.58	0.300	118.43-118.73	2.4/2.62	24.1
9	184.41	2.000	183.41-185.41	1.5/1.87	16.1
10	186.51	2.000	185.51-187.51	1.5/1.87	16.1
11	190.31	2.000	189.31-191.31	1.5/1.87	16.1
12	204.8	2.000	203.8-205.8	1.4/1.76	15.2

The receiver architecture consists of two separate receiver chains. A simplified payload block diagram is shown in Figure 2. The W- and F-band channels (i.e., Chan. 1 through 8) are implemented with a superheterodyne radiometer. The W-band channel is double sideband, and the F-band channels are single sideband. The W/F receiver has a local oscillator with a fundamental frequency of 30.552 GHz. The G-band channels are implemented with a direct-detect radiometer using single sidebands.

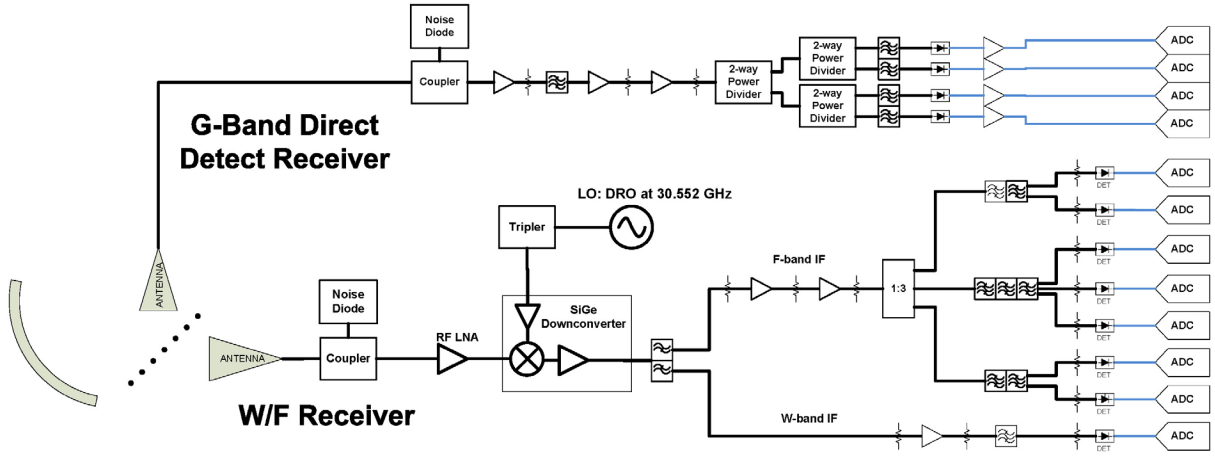

Figure 2 Simplified TROPICS payload block diagram

4.2 Spatial Response

Figure 2 also has a simple illustration of the antenna subsystem. Inside the payload is an offset parabolic reflector with separate feedhorns for the W/F-band receiver and the G-band receiver. The feedhorns illuminate the reflector through a wire gird polarizer, which allow the incoming radiation to be diplexed. More information on polarization is in Sect. 4.3. Figure 3 is an illustration of the TROPICS cross-track scan. The scan is implemented by spinning the entire payload "cube" in reference to the spacecraft bus. Similar to a conical scanner, TROPICS uses a motor and slipring to rotate the payload, but in a cross-track scan pattern on the surface. Table 2 contains the scan

pattern details for the cross-track swath projected beneath the space vehicle. There are 81 spots or beam positions in the Earth View Sector. TROPICS scans during the integration period; therefore, the cross-track dimension will be larger than the down-track dimension. Due to the wire grid, the TROPICS footprints will have minimal offset on the ground, which is a tremendous advantage in post-processing. Sect. 1 has a table of the dimensions of each footprint separated out by band (W, F, G, and 205 GHz) and track. To compare the swath width to ATMS, Figure 4 plots the footprints of the spots on the Earth's surface, along with the ATMS footprints.

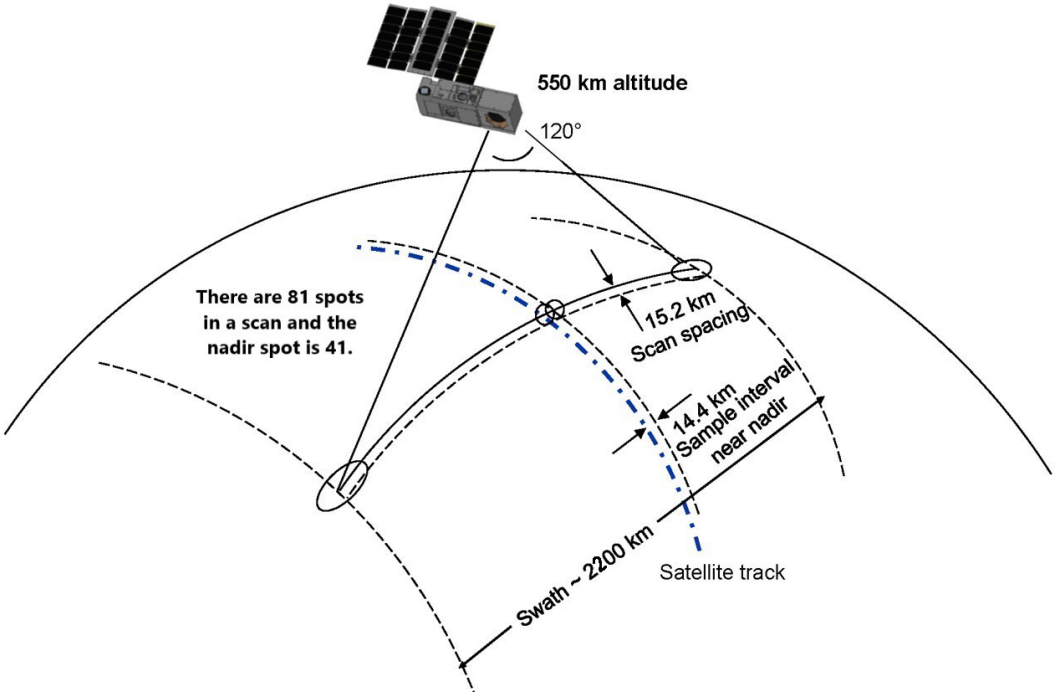

Figure 3 Illustration of the TROPICS cross-track scan pattern.

Table 2 TROPICS scan profile characteristics

Characteristic	Units	Value
Rotation Period	Seconds	2
Maximum Earth View Sector Angle	Degrees	± 60
Scan Type	N/A	Constant velocity (scanning during integration)
Integration time	Seconds	1/120
Number of Earth View Sector Measurements	N/A	81 per scan (one at nadir)

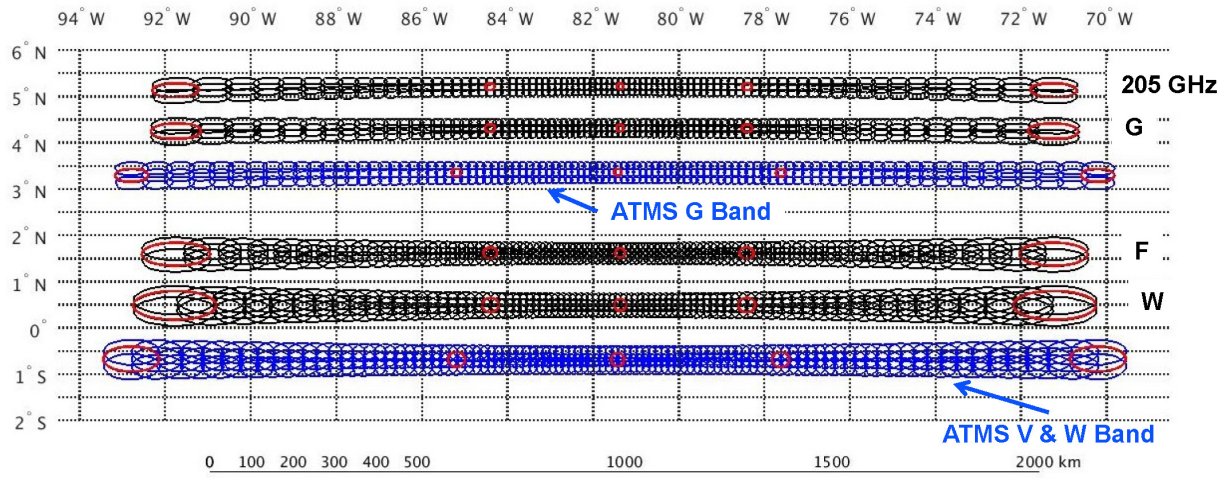

Figure 4 TROPICS swath comparison against ATMS. TROPICS' altitude for this rendering was 550 km.

4.3 Polarization

As previously mentioned, the TROPICS payload has a non-traditional polarization. Figure 5 illustrates the TROPICS polarization, which is a combination of the traditional conical scanner (i.e., fixed angle between reflector and feedhorn) and the cross-track scanner (i.e., scan angle to zenith angle conversion at the surface). As illustrated in the upper left-hand side, the polarization is fixed for the W/F band at 70 deg. (i.e., Phi, φ, in the figure, which is called the polarization angle), while the G-band will be -20 deg. per the angle φ defined in the figure. This makes the polarization largely the same as the upwelling horizontal and vertical polarization. This is true for all bands. The polarization was measured pre-launch in an antenna range, with W/F band at 70 deg. and G-band at -20 deg., but post-launch assessment of the Pathfinder data derived an empirical W/F-band angle of 0 deg. and G-band at 90 deg. The mixing equation is in Equation 1. Phi, φ, is typically the scan angle in traditional cross-track radiometers, but the TROPICS feedhorn moves

Equation 1 $$T_b = T_b^{hori} * cos^2(\varphi) + T_b^{vert} * sin^2(\varphi)$$

with the reflector (and the entire payload) and therefore remains constant while the entire payload rotates. In the spaceborne radiative transfer equation (not shown), the polarized sources of radiation for the TROPICS instrument is the ocean surface, while the atmosphere and land are largely unpolarized.

Figure 6 is a simulation of the ocean emissivity versus instrument scan angle. The solid black and blue lines are the surface emissivity's vertical and horizontal components, respectively. The solid green is the mixed polarization where the polarization angle is 0 deg. (i.e., horizontal emissivity) for the TROPICS W/F receiver (Channel 1). For Channel 12 (G-band), the solid green is the mixed

polarization where the polarization angle is 90 deg. (i.e., vertical emissivity). For comparison, the typical cross-track "quasi" polarization, which has the same equation as Equation 1, but with Phi, i.e., the polarization angle, replaced with the changing scan angle.

Finally, Figure 7 shows an idealized simulated brightness temperature as a function of scan angle with the fixed 0/90 deg. polarization angle (W & F/G) for a tropical ocean surface. There is limb darkening or brightening due to the change in thickness of the atmosphere and surface emissivity. This simulation does not model antenna pattern sidelobes (i.e., it is a Gaussian beam).

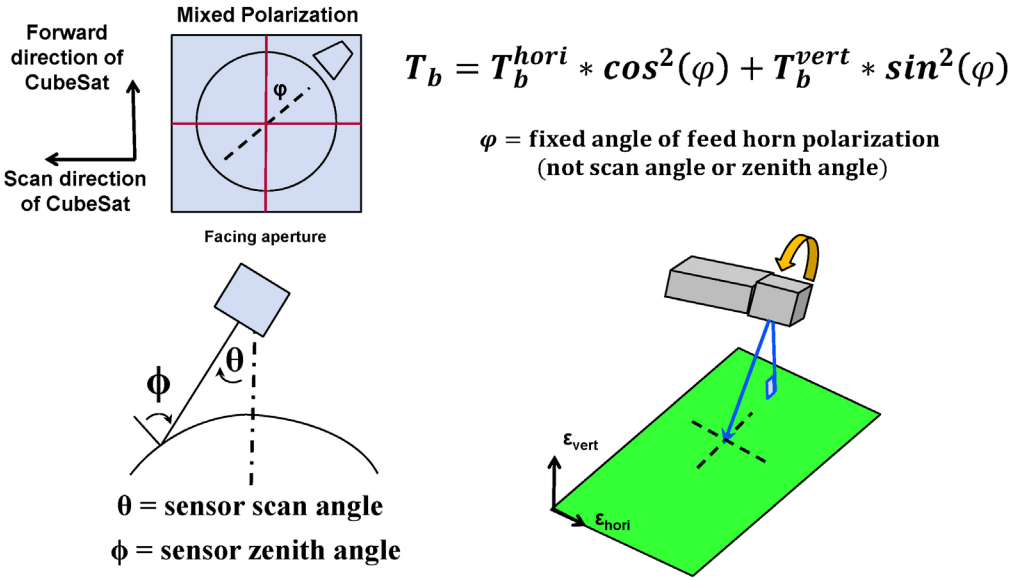

Figure 5 Illustration explaining the TROPICS polarization.

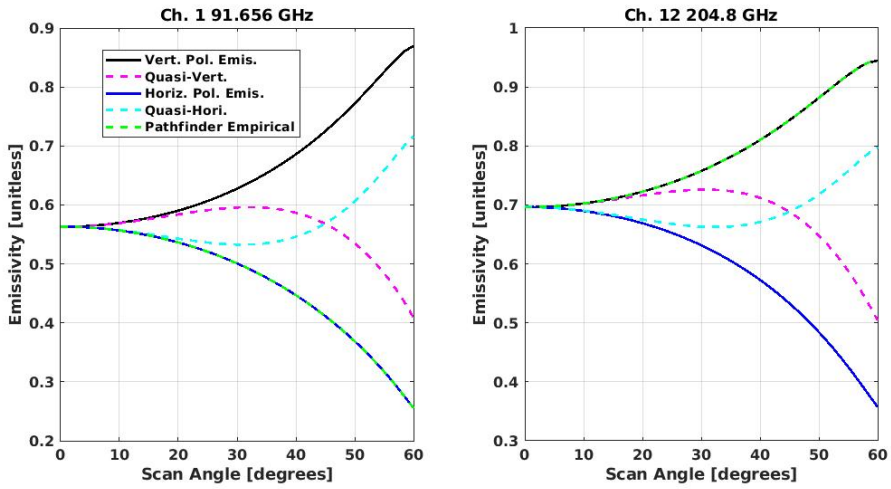

Figure 6 Simulated ocean surface emissivity (fastem v2)

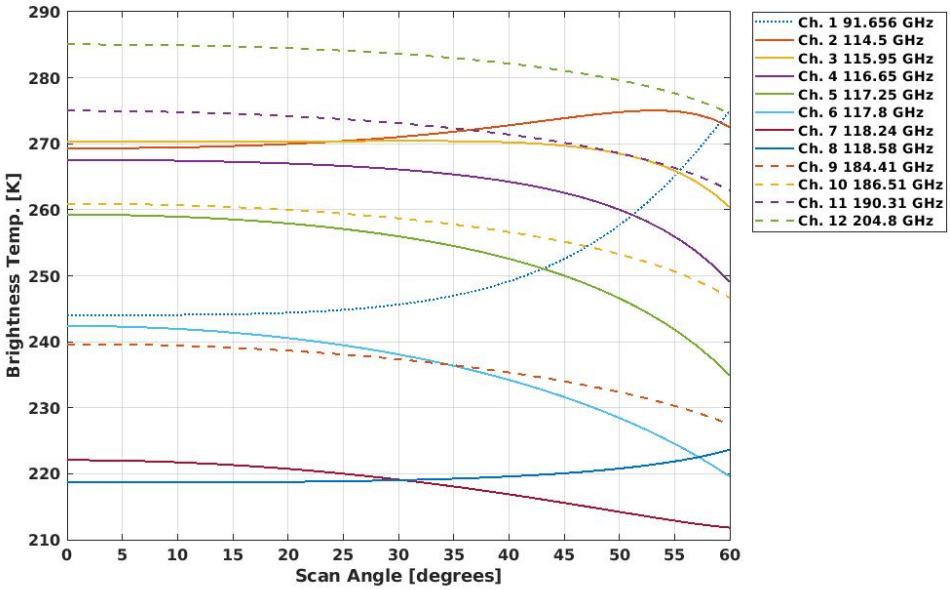

Figure 7 Simulated brightness temperature vs sensor scan angle from the tropical US Standard 1976 atmosphere and fastem version 2 ocean emissivity model. W/F-band at 0 deg. and G-band at 90 deg.

5 Data Products

A comprehensive data product description can be found in the TROPICS Data User's Guide. A high-level description of the data products are given in Table 3.

Table 3 TROPICS data product descriptions

Level Designation	Data Product Description
Level 0	raw CCSDS payload and telemetry from space vehicles
Level 1a	Timestamped, geolocated, calibrated antenna temperature
Level 1b	Timestamped, geolocated, calibrated brightness temperature with bias removed
Level 2a URRP	Spatially resampled (i.e., collocated) brightness temperature (F-band resolution)
Level 2b	Atmospheric Vertical Temperature Profile [Kelvin]
	Atmospheric Vertical Moisture Profile Profile [g/g]
	Instantaneous Surface Rain Rate [mm/hr]
	TC Intensity: Mean Sea-level pressure [mb]
	TC Intensity: Maximum Sustained Wind [m/s]

6 URRP Algorithm Description

6.1 Objective of L2A-URRP

The objective of the L2A-URRP product is two-fold:

- The first objective is to provide G-band brightness temperatures that match the spatial resolution of F-band. These brightness temperatures can be used in T/q retrievals and should improve those retrievals in two ways:
  - The resolution matching provided in L2A-URRP has both bands see the same scene, rather than G-band having a higher resolution. Thus, retrievals should be more consistent.
  - The Backus-Gilbert averaging described below will be performed on the G-band channels. This will reduce sensor noise and thereby reduce a-posteriori uncertainty in the retrieved q-profiles. The noise reduction factor is reported in the retrievals.
- The second objective is to provide a measure for the atmospheric inhomogeneity within an observed footprint. For this purpose, a Backus-Gilbert-weighted standard deviation of Channel 12 is also reported in the Level 2A product.

Figure 2 shows a simulated TROPICS scan geometry for different positions within the swath. One can see that the 3dB footprint width of the G-band channels is considerably narrower than that of the F-band channels. This provides opportunities for the aforementioned averaging as well as for calculating the variability within the wider F-band footprint.

The remainder of the document is structured as follows: First, we discuss the Backus-Gilbert method in general. Next, we discuss its application to TROPICS and finally, we assess its performance based on Hurricane Nature Run simulations.

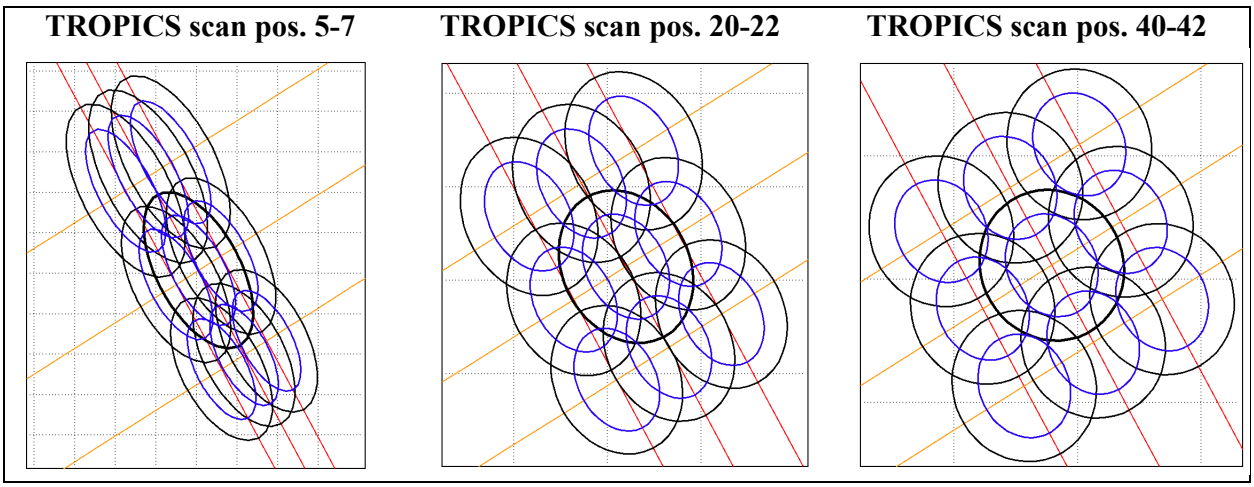

Figure 8: TROPICS scan patterns for scan positions 5-7 (near scan edge, left panel) and 20-22 (halfway out from the scan center, middle panel) and 40-42 (center of scan, right panel) for three consecutive scans. The blue ellipses are the 3dB effective fields of view for the TROPICS G-Band channels near 183 GHz. The black

ellipses are the 3dB effective fields of view for the TROPICS F-Band channels near 118 GHz. The center of the 3x3 footprint field is highlighted bold. The red lines show the scan direction of the three scans and the yellow lines connect identical scan positions between adjacent scan lines. The dotted grid is equally spaced with a grid size of 20 km in latitude and longitude direction. Note that the fields of view are much larger and more elliptical for the off-nadir observations (left panel).

6.2 The Backus-Gilbert Method

The Backus-Gilbert (BG) method (Backus and Gilbert, 1970) provides a regularized way of remapping geophysical observations to a pre-described target resolution. The BG-method has been used relatively extensively in microwave remote sensing for three purposes:

- Deconvolution: The method is used to enhance the resolution of oversampled passive microwave observations. A deconvolution can be thought of a high-pass filter that enhances resolution and at the same time increases sensor noise. Examples for the application of this method are Bauer and Bennartz (1998) and, more recently, Petty and Bennartz (2016) as well as references therein. As outlined in both of these publications, high-pass filters inevitable create 'negative' side-lobes in the process.
- Convolution: The BG-method can also be used for convolution, which degrades the resolution of the observations to a previously defined target resolution. An example for convolution is given in Bennartz (2000), where high-resolution AMSU-B observations are averaged to match the spatial sensitivity of lower-resolution AMSU-A observations. The process of convolution typically reduces noise.
- Optimal interpolation: Poe (1990) have successfully used the Backus-Gilbert method to interpolate observations under controlled conditions. That is, if the footprint center location of the observations lies at an undesirable position, the BG-method can be used to create a synthetic observation lies between the actually observed footprints. The advantage of the BG-method over other interpolation methods is that the antenna pattern of the shifted footprint can be optimized in the process.

The BG-method typically works by taking a number of N × M observations surrounding a central observation, which is to be corrected. The BG-method then provides mathematical method for finding weights a_i, so that:

$$T_{BG} = \sum_{i=1}^{N \times M} a_i \cdot T_i \tag{1}$$

The weights depend on the antenna patterns of the input temperatures (T_i) and the desired spatial sensitivity of the target observation (T_{BG}) but not on the scene that is actually observed. In addition, a tuning parameter exists that allows for a trade-off between the goodness of fit and the noise amplification when the weights are derived. The cost function Q and tuning parameter γ used here are identical to the cost function reported in Bauer and Bennartz (1998), see Equations (3) to (5) therein.

The a_i-s are constrained so that:

$$\sum_{i=1}^{N\times M} a_i = 1 \tag{2}$$

The noise amplification *e*, importantly, follows straight from Gaussian error propagation to be:

$$e = \sqrt{\sum_{i=1}^{N\times M} a_i^2} \tag{3}$$

Thus, if all $a_{i\text{-}s}$ are positive and smaller than one, it follows that $e<1$ and the noise is reduced. This is the case for convolution applications. For deconvolution applications, some a_i are typically larger than one so that $e>1$ and the noise of T_{BG} will be enhanced. A full discussion of these issues as well as a full mathematical description of the BG-method is given both in Bauer and Bennartz (1998) and in Petty and Bennartz (2016).

6.2.1 Derivation of BG-weights

The general relation between noise amplification e and the tuning parameter γ is shown in Figure 3. As the tuning parameter increases to its maximum value of 90 degrees, the noise amplification decreases, corresponding to a weighted average at larger values of the tuning parameter. For an exact value of 90 degrees, the BG method returns equally weighted averaging. For small very values of the tuning parameter the BG solution becomes unstable and yields arbitrarily high noise amplifications. For the particular example shown in Figure 3, this would be for values of $\gamma < 8$. While the principal shape of the curve shown in Figure 3 remains the same, its actual shape will vary with the size (*NxM*) of the BG window and the chosen target APF.

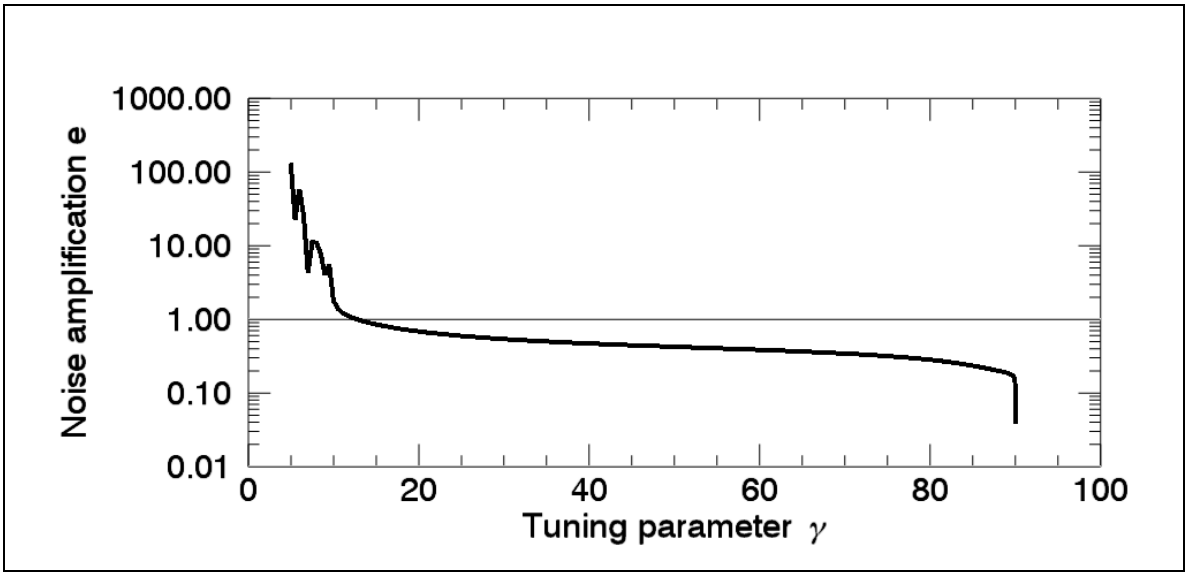

Figure 9: This figure illustrates the principal relation between tuning parameter and noise amplification.

Bauer and Bennartz (1998) examine the goodness of the BG reconstruction of the target APF using the noise amplification e and the 'integral difference to the target APF'. Using the same notation as Bauer and Bennartz (1998) this latter quantity is defined as:

$$\sigma_2 = 50 \cdot \int_X \int_Y \left| G_T(x,y) - \sum_{i=1}^{N \cdot M} a_i \cdot G_{EFOV,i}(x,y) \right| dx\,dy \tag{4}$$

This quantity provides a measure for how different the target APF (G_T) and the BG-weighted reconstructed APFs are in an absolute sense. If both were identical, then the integral would be zero. If both were completely different, then the integral would be two and the resulting value $\sigma_2 = 100$. This can be interpreted as a %-agreement value.

Subsequently, we describe how the BG-Method is applied to convolve the TROPICS G-Band to F-Band and which parameters will be reported in the L2A-URRP product. We further briefly discuss possible deconvolution strategies, which are however found to be not viable in the framework TROPICS.

6.3 Optimal Convolution of TROPICS G-band to F-band

Figure 4 and Figure 5 show the results of an optimal convolution of the TROPICS G-band to F-band. Optimal weights for the convolution are by example presented for three TROPICS scan positions 5, 20, and 40. The noise amplification and integral difference are optimal, if $\gamma \to 0$ and they do not depend on size of averaging area as long as it is at least 5×5. Thus, a 5×5 averaging area appears optimal for the purpose of this product.

Figure 5 shows cross-sections for reconstructed APFs for a box size of 5x5 and σ_2=0. As expected, the reconstructed F-Band (blue) spatial sensitivity matches the true F-band (red) spatial sensitivity in a very good manner. Noise amplification is around 0.3-0.4 depending on scan position, thus reducing the already low G-band noise even further.

These results are consistent with expectations for example based on earlier studies using AMSU-A and AMSU-B (Bennartz, 2000) and highlight the value of such a convolution in matching resolution between different bands with different resolution.

In addition to the convolved brightness temperature product we are also planning to provide an optimally weighted spatial standard deviation at Channel 12 (205 GHz). This product can be used to identify inhomogeneous scenes at F-band that might be caused for example by precipitation within the field of view. We envision such information can be useful in determining environmental condition for example when retrieving temperature and water vapor profiles.

The optimally weighted spatial standard deviation product will be calculated as follows:

$$\Delta T_{BG} = \sqrt{\sum_{i=1}^{N\times M} a_i^2 \cdot \left(T_i - T_{BG}\right)^2} \tag{5}$$

where ΔT_{BG} refers to the spatial standard deviation of brightness temperatures and T_{BG} refers to the reconstructed brightness temperature calculated using Equation (1). We are currently planning to provide ΔT_{BG} only for Channel 12 as this is the only G-Band window channel and it will have the strongest spatial variability.

6.3.1 Finding the optimal weights a_i for TROPICS URRP

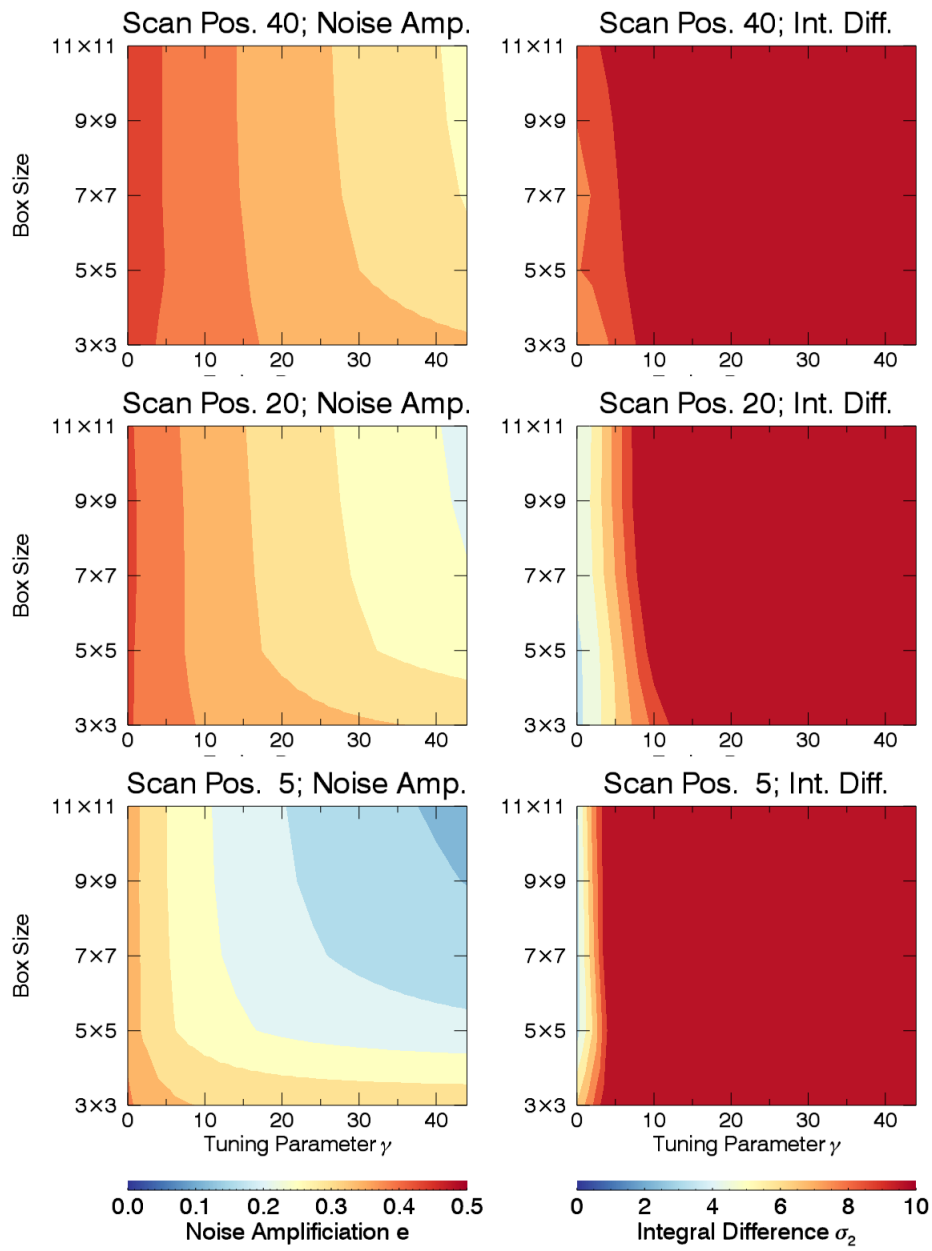

Figure 10: BG-results for convolution of G-band to F band in terms of noise amplification (*e*, left panels) and integral difference between source and target APF (σ_2, right panels) for three TROPICS scan positions as function of box-averaging size and tuning parameter (γ).

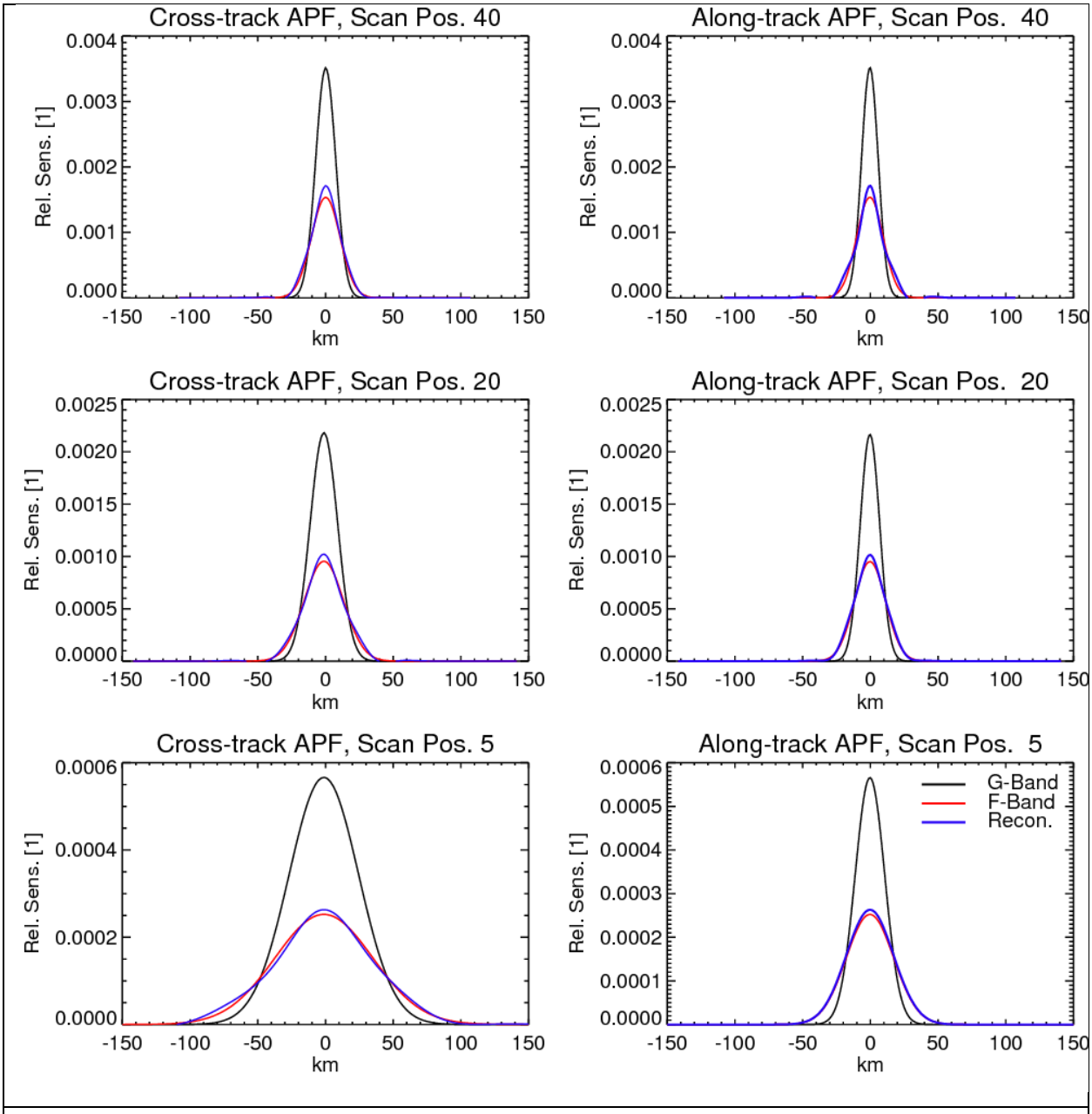

Figure 11: BG-results for convolution of G-band to F band. Shown are cross-sections of the G-band and F-band APFs as well as the BG-reconstructed APF for a box size of 5x5 and γ =0.

6.3.2 Possibility of deconvolution of F-Band to higher spatial resolution

For completeness we provide here the results of a possible spatial deconvolution in which the F-band brightness temperatures are deconvolved to the higher G-band resolution. The results summarized here indicate this is not a viable solution for TROPICS as the spatial oversampling is not high enough to provide enough information for a meaningful spatial deconvolution. Indeed, earlier studies have shown that even for highly oversampled sensors, such as the TMI 10 GHz channel, the potential value of deconvolution is somewhat limited (Petty and Bennartz, 2017; Bauer and Bennartz, 1998).

Figure 6 and Figure 7 summarize the results for TROPICS. Weights for the deconvolution were found for three scan positions 5, 20, and 40. Figure 6 shows noise amplification and integral difference as function of box size and γ. The noise amplification and integral difference vary widely with γ, and especially high values of γ yield large values for noise amplification.

Even for those large noise amplifications, integral difference cannot be made smaller than σ_2=25 without unacceptably high noise amplification. For comparison, the integral difference between the original G-Band and F-band APFs is σ_2=29. Thus, even allowing for large noise amplification, the deconvolved APF does not represent the target G-band APF much better than original F-Band APF.

As an example for this behavior, Figure 7 shows cross-sections for reconstructed APFs for a box size of 5x5 and a σ_2 chosen so that noise amplification is around e=1.5 in all cases. One can see that the deconvolved APF (blue) lies between the original (black) and target (red) APF but resembles the original APF still better than the target APF. One can also identify the typical negative sidelobe that occur because the BG-method realizes a high-pass filter in the case of deconvolution. Those negative side-lobes are also reported in earlier studies (e.g. Petty and Bennartz, 2017; Bauer and Bennartz, 1998). In addition to a non-optimal fit, the application of the deconvolution would also increase the F-band noise by a factor of e=1.5, which is undesirable also for temperature and moisture retrievals.

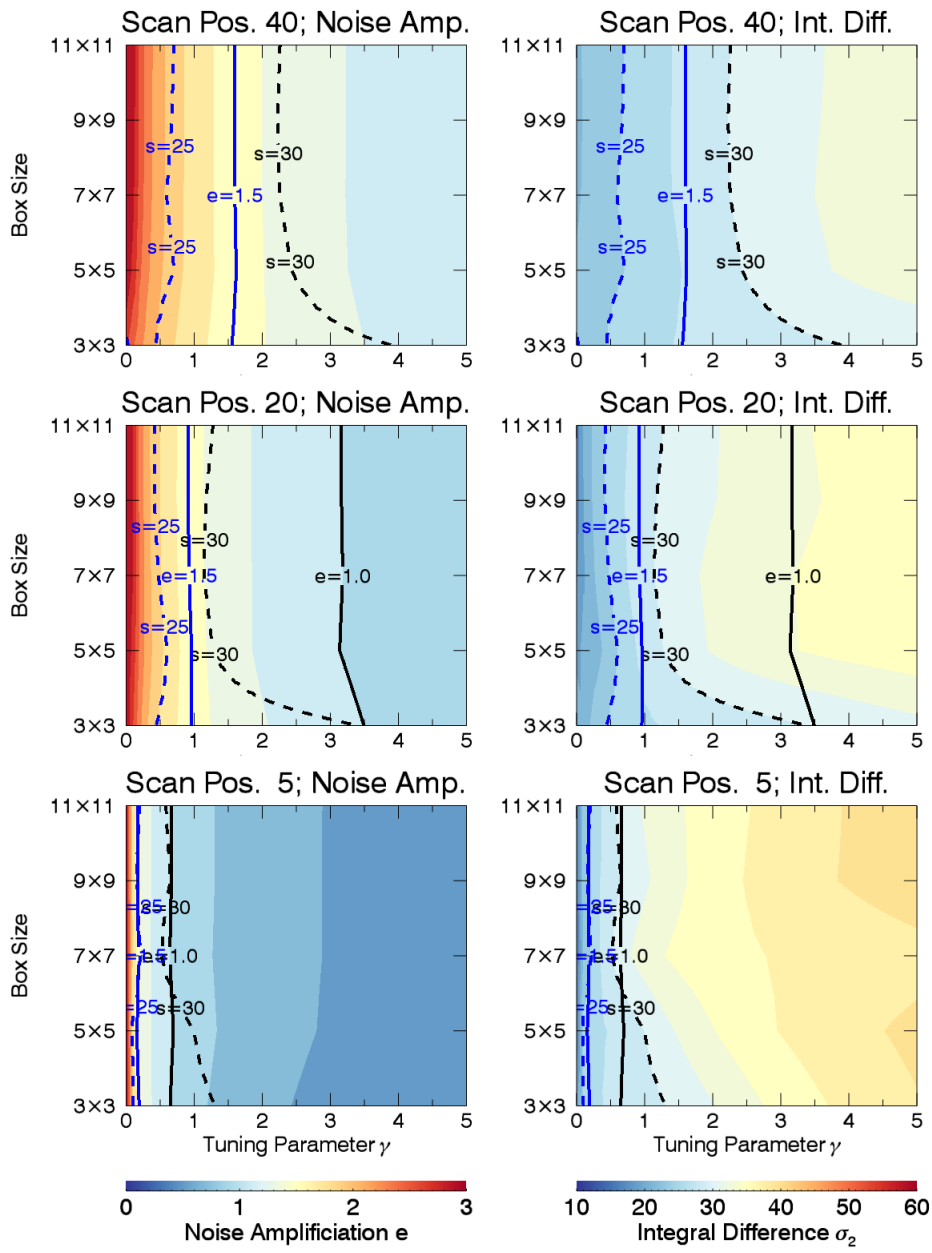

Figure 12: Same as Figure 4 but for deconvolution of F-band to G-band. In addition lines of isolines of constant e (at e=1.0, e=1.5) and σ_2 (at σ_2=30 and σ_2=25) are shown. Note, the scales of the color bars are different from Figure 4.

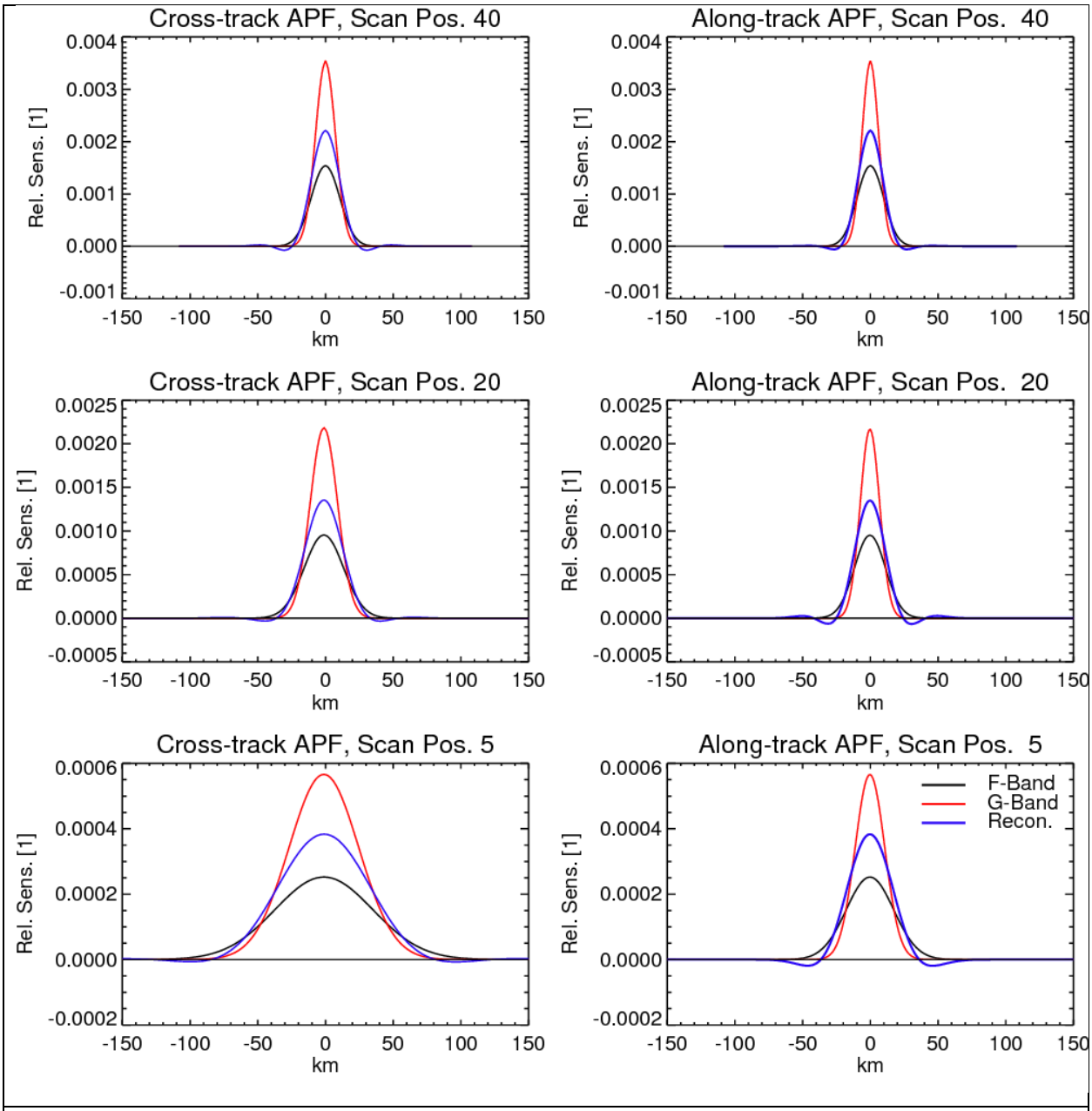

Figure 13: BG-results for deconvolution of F-band to G-band. Shown are cross-sections of the G-band and F-band APFs as well as the BG-reconstructed APF for a box size of 5x5 and for variable values of σ_2, so that the noise amplification is about e=1.5 in all cases.

6.3.3 Radiometric Products Reported in L2A-URRP

The L2A-URRP provides similar file structures and information as Level 1b. In addition to all information available at Level-1b, it will report the G-Band brightness temperatures matched to F-Band resolution, described in Section 6.3 as well as a measure for the spatial standard deviation of 205 GHz brightness temperatures within each F-band footprint. A list of products reported in L2A-URRP is compiled in Table 4.

Table 4: Overview of products reported on L2A-URRP.

	Name	Resolution	Comment
Navigation and housekeeping Information	Same as in Level 1b	Native resolution	These are the same as reported in Level 1b.
Channel 1-12	TEMPBRIGHT_L2A	Native Resolution	These are the same as reported in Level 1b.
Channel 9-12	TEMPBRIGHT_L2A	Channels 1-8 at their native resolution, Channels 9-12 Convolved to F-Band resolution	These are channels 9-12 convolved to match F-Band resolution. See Section 6.3. Channels 1-8 are also provided but are not modified from the L1b product.
Channel 12 Standard deviation	STDDEV_CH12_L2A	Channel 12 Standard deviation.	Standard deviation of channel 12 within a F-Band footprint using Backus-Gilbert weighting. See Section 6.3.
Noise Reduction	NOISE_REDUCTION_L2A	Channels 1-8 at their native resolution, Channels 9-12 Convolved to F-Band resolution	Noise reduction for all channels. Note, this value is one for Channels 1-8, which are not modified from L1b. Only channels 9-12 have reduced noise.

7 Performance Assessment

Product performance has been assessed in the above Section 6.3. Here we use simulated Hurricane Nature run data to further assess the performance of the product for realistic scenes. Figure

8 below shows an example of the BG-method applied to one simulated TROPICS HNR case. One can see that:

1. In regions near the hurricane, the difference between the convolved L2a brightness temperatures and the L1b brightness temperatures can exceed ±10 K.
2. The Channel-12 standard deviation highlights areas, where the atmosphere is particularly inhomogeneous at scales relevant for the passive microwave remote sensing. This parameter can help identify regions with deep convection.
3. In addition, the noise amplification is typically between 0.3 and 0.6, thus effectively reducing any random G-band noise (NEDT) by a factor of 0.3 to 0.6. This reduction in noise will lead to improved moisture retrieval accuracy, if the Level-2a data is used instead of the Level-1b in the T/q retrievals.
4. Note that toward the scan edge the noise reduction is not as good as further inside the scan because the F-band field of view cannot be reconstructed as well as in the inner parts of the scan. This is simply because the target footprint (being at the edge of the scan itself) cannot be centered into a 5x5 box of surrounding pixels.

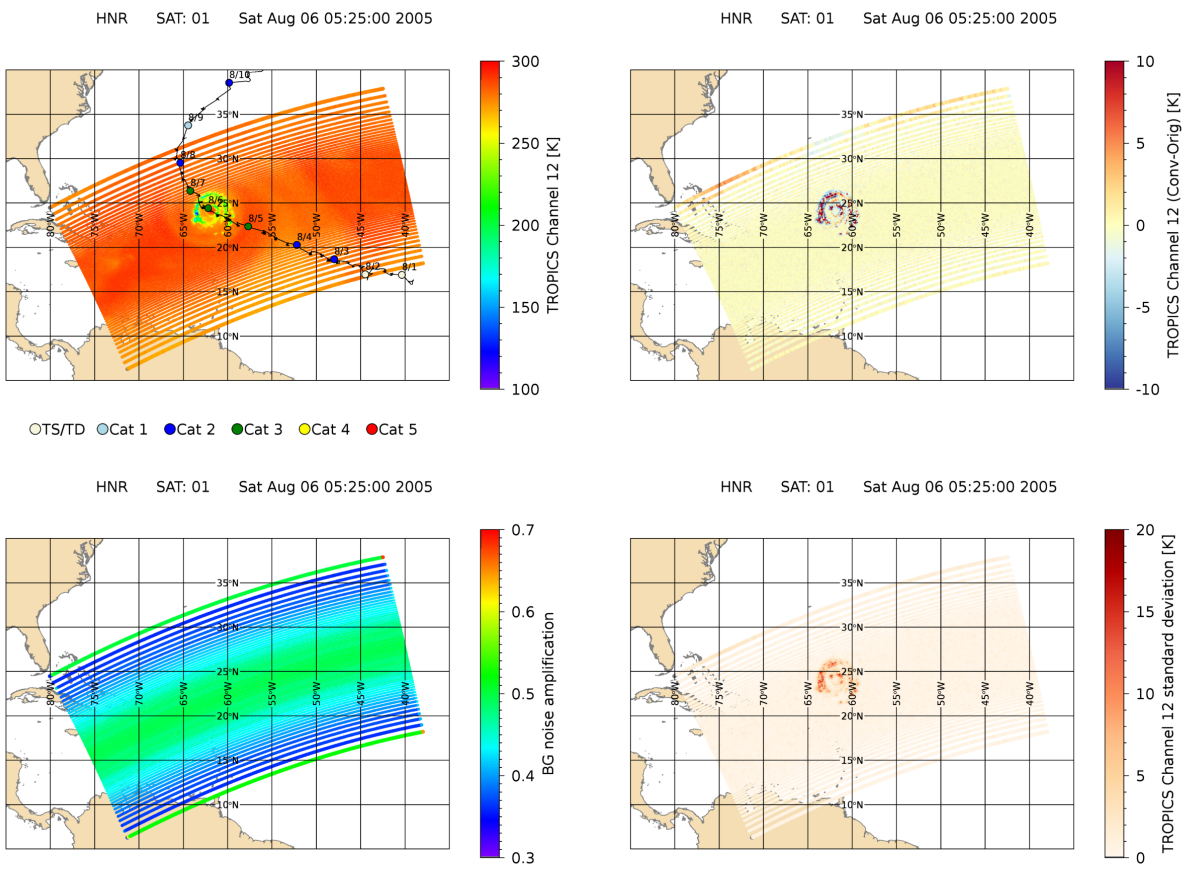

Figure 14: Example of BG-averaging applied to one simulated L1b TROPICS Hurricane Nature Run (HNR) granule. The upper left panel shows the simulated L1b brightness temperature for Channel 12. The upper right panel shows the difference between the BG-convolved L2A brightness temperature and the L1A brightness temperature. The lower left panel shows the noise amplification, values lower than one meaning that the noise is actually reduced. The lower right panel shows the BG-weighted standard deviation of Channel 12 following Equation (5) .

8 References

Backus, G., and Gilbert, F.: UNIQUENESS IN INVERSION OF INACCURATE GROSS EARTH DATA, Philosophical Transactions of the Royal Society of London Series a-Mathematical and Physical Sciences, 266, 123-&, 10.1098/rsta.1970.0005, 1970.

Bauer, P., and Bennartz, R.: Tropical Rainfall Measuring Mission microwave imaging capabilities for the observation of rain clouds, Radio Sci, 33, 335-349, 10.1029/97rs02049, 1998.

Bennartz, R.: Optimal convolution of AMSU-B to AMSU-A, Journal of Atmospheric and Oceanic Technology, 17, 1215-1225, 10.1175/1520-0426(2000)017<1215:ocoabt>2.0.co;2, 2000.

Petty, G. W., and Bennartz, R.: Field-of-view characteristics and resolution matching for the Global Precipitation Measurement (GPM) Microwave Imager (GMI), Atmospheric Measurement Techniques, 10, 745-758, 10.5194/amt-10-745-2017, 2016.

Poe, G. A., 1990: Optimum interpolation of imaging microwave radiometer data. IEEE Trans. Geosci. Remote Sens., 28, 800–810.